Chemical Science

ROYAL SOCIETY OF CHEMISTRY

EDGE ARTICLE

View Article Online
View Journal | View Issue

Cite this: *Chem. Sci.*, 2022, **13**, 2475

All publication charges for this article have been paid for by the Royal Society of Chemistry

Arene–perfluoroarene interactions confer enhanced mechanical properties to synthetic nanotubes†

Emily K. Roesner, [a] Darya Asheghali, [b] Alina Kirillova, [c] Michael J. Strauss, [a] Austin M. Evans,[a] Matthew L. Becker *[bcde] and William R. Dichtel *[a]

Supramolecular nanotubes prepared through macrocycle assembly offer unique properties that stem from their long-range order, structural predictability, and tunable microenvironments. However, assemblies that rely on weak non-covalent interactions often have limited aspect ratios and poor mechanical integrity, which diminish their utility. Here pentagonal imine-linked macrocycles are prepared by condensing a pyridine-containing diamine and either terephthalaldehyde or 2,3,5,6-tetrafluoroterephthalaldehyde. Atomic force microscopy and synchrotron *in solvo* X-ray diffraction demonstrate that protonation of the pyridine groups drives assembly into high-aspect ratio nanotube assemblies. A 1 : 1 mixture of each macrocycle yielded nanotubes with enhanced crystallinity upon protonation. UV-Vis and fluorescence spectroscopy indicate that nanotubes containing both arene and perfluoroarene subunits display spectroscopic signatures of arene–perfluoroarene interactions. Touch-spun polymeric fibers containing assembled nanotubes prepared from the perhydro- or perfluorinated macrocycles exhibited Young's moduli of 1.09 and 0.49 GPa, respectively. Fibers containing nanotube assemblies reinforced by arene–perfluoroarene interactions yielded a 93% increase in the Young's modulus over the perhydro derivative, up to 2.1 GPa. These findings demonstrate that tuning the chemical composition of the monomeric macrocycles can have profound effects on the mechanical strength of the resulting assemblies. More broadly, these results will inspire future studies into tuning orthogonal non-covalent interactions between macrocycles to yield nanotubes with emergent functions and technological potential.

Received 27th October 2021
Accepted 28th January 2022

DOI: 10.1039/d1sc05932g

rsc.li/chemical-science

Introduction

Supramolecular polymerization of macrocycles[1–6] offers a means to design nanotubes with distinct interior environments for chemical separations,[7,8] selective ion transport,[9–11] energy storage,[12,13] or size-selective catalysis.[14,15] However, many of these assemblies rely on weak cohesive interactions that are disrupted by minor structural variations, elevated temperatures, or mechanical stress.[16–18] Assemblies that form reliably and under a broad range of conditions, while retaining their stimuli-responsive nature will offer utility in a wide range of applications. Recently, we found that imine-linked macrocycles with 1–4 nm diameters form high-aspect ratio nanotubes upon protonation of their interior basic groups.[19] Protonation establishes strong yet reversible electrostatic and solvophobic forces that produce assemblies with mechanical strengths that rival covalent polymers and biological filaments.[20] These designs have since been generalized to incorporate many dialdehyde residues by designing a universal diamine monomer based on a 2,6-diarylpyridine motif.[21] With this approach, the properties of synthetic nanotubes can now be improved by chemical design. In this report, we demonstrate how the Young's modulus of nanotube-derived fibers can be increased by incorporating strong arene–perfluoroarene interactions into their macrocycle building blocks. Because their mechanical properties emerge from a noncovalent assembly that is acid-responsive, these strong fibers can be disassembled, and the macrocycles recovered by treatment with base.

Arene–perfluoroarene (AP) interactions arise between highly fluorinated aromatic systems and their analogous hydrogen-containing counterparts. The electronegative fluorine atoms invert the classically negative quadrupole moment of aromatic compounds, which can induce or direct alternating stacking of opposite quadrupole vectors.[22] AP interactions have been used to direct or influence solid-state packing and molecular organization,[23–26] including to stabilize liquid crystalline phases,[27–29]

[a]*Department of Chemistry, Northwestern University, Evanston, IL 60208, USA. E-mail: wdichtel@northwestern.edu*

[b]*Department of Chemistry, Duke University, Durham, NC 27708, USA. E-mail: matthew.l.becker@duke.edu*

[c]*Thomas Lord Department of Mechanical Engineering and Materials Science, Duke University, Durham, NC 27708, USA*

[d]*Department of Biomedical Engineering, Duke University, Durham, NC 27708, USA*

[e]*Department of Orthopedic Surgery, Duke University, Durham, NC 27708, USA*

† Electronic supplementary information (ESI) available. See DOI: 10.1039/d1sc05932g

direct topochemical polymerizations,[30] and enhance electronic communication within noncovalent assemblies.[31–34] Here, we explore their ability to impart additional strength to macrocycle assemblies by assembling two pentagonal macrocycles derived from diamine, **1**, condensed with either terephthalaldehyde (**2**) or its perfluorinated analogue (**3**, Fig. 1). Both macrocycles separately assemble into high-aspect ratio nanotubes upon protonation, as evident by atomic force microscopy (AFM) and synchrotron *in solvo* X-ray diffraction (XRD). However, upon protonation, a 1 : 1 stoichiometric mixture of the macrocycles assembles into nanotubes with enhanced crystallinity due to AP interactions that reinforce the structure. Touch-spinning fibers from solutions of each nanotube type provided insight into the effects of AP interactions on the nanotube's mechanical properties. Nanotube-loaded (99 wt%) fibers supported by AP interactions exhibited Young's moduli of 2.1 GPa, a 93% increase relative to those of nanotube fibers bearing solely aromatic or perfluoroaromatic residues, 1.09 and 0.49 GPa, respectively. These findings demonstrate that AP interactions are a powerful tool in constructing robust nanomaterials and represent the first example of directly comparing the mechanical effects of AP interactions on supramolecular assemblies to analogous non-AP assembled systems. More broadly, this work highlights how coupled synthetic design and nanoscale assembly can be used to construct materials with useful properties.

Results and discussion

NT1 and **NT2** are each synthesized in a single step by condensing the 2,4,6-triphenylpyridine-based diamine (**1**) with either terephthalaldehyde (**2**) or 2,3,5,6-tetrafluoroterephthalaldehyde (**3**) in the presence of CF_3CO_2H (0.5 equiv. relative to **1**) as a catalyst. In addition to catalyzing imine formation and exchange, the acid protonates the pyridine group of **1** and its condensed products. Electrostatic interactions between co-assembled cationic macrocycles and $CF_3CO_2^-$ drives assembly into nanotubes, which are further stabilized by secondary solvophobic interactions from the aliphatic side chains. This one pot synthesis results in high yields of macrocycle formation relative to other potential imine-linked products.[35,36] Neutral, monomeric [5 + 5] imine-linked macrocycles (**MC1** and **MC2**, respectively) are isolated in high yields (81% each) from these gelled reaction mixtures after neutralization with triethylamine, isolation by centrifugation, and subsequent washing with solvents in which the macrocycles are not soluble (see ESI† for detailed synthesis and purification procedures).[21] The neutral macrocycles were then characterized by matrix-assisted laser desorption/ionization time of flight mass spectrometry (MALDI-TOF MS), size exclusion chromatography (SEC), and ^{1}H NMR spectroscopy. SEC of both macrocycles showed a single narrow elution band consistent with the formation of single macrocyclic products (Fig. 2A). MALDI-TOF MS exclusively provided the expected $[M + H]^+$ adducts at 2958.23 *m*/*z* and 3317.87 *m*/*z* for **MC1** and **MC2**, respectively (Fig. 2B). In both cases, no oligomeric species, which have substantially higher ionization efficiencies than the macrocycles were observed. Both macrocycles exhibited a ^{1}H NMR spectrum consisting of well-defined resonances that are consistent with a symmetric macrocycle (Fig. S5 and S6†). **MC1** was soluble in a variety of organic solvents, yielding a ^{1}H NMR spectrum with no resonances corresponding to free aldehydes (*ca.* 10 ppm) or amines (*ca.* 5.5 ppm), further validating the macrocyclic structure. The lower solubility of **MC2** required long sonication times to obtain a ^{1}H NMR spectrum with

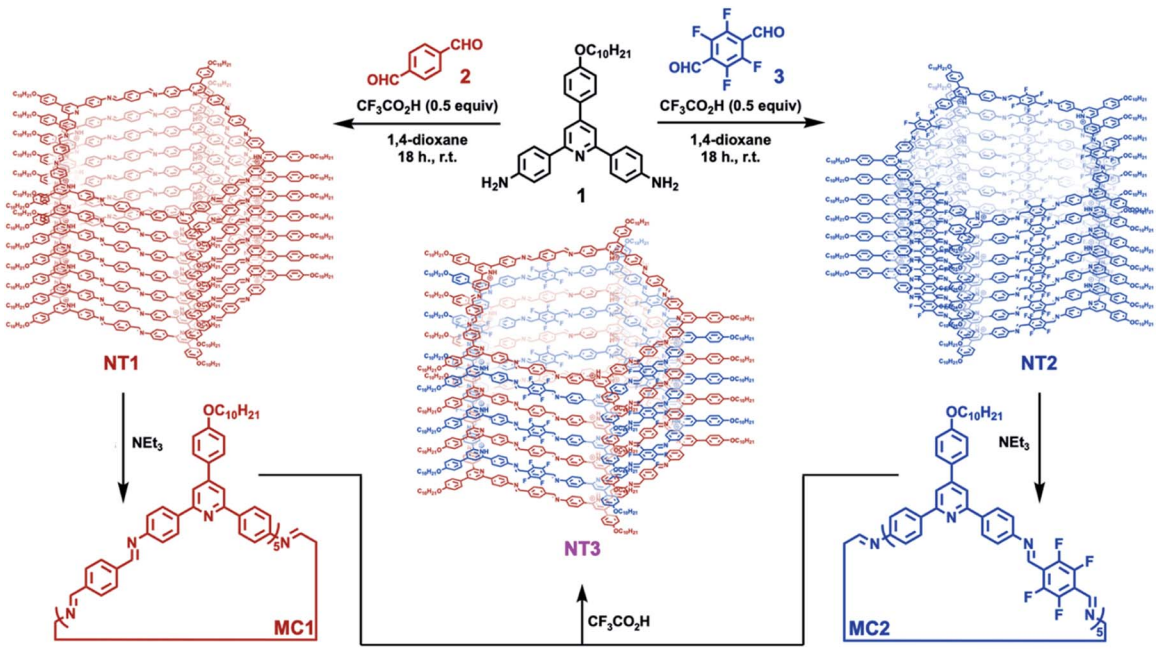

Fig. 1 Synthesis of pentagonal [5 + 5] imine-linked macrocycles and their assembly into the corresponding nanotube, along with an alternating nanotube prepared from a binary mixture of macrocycles.

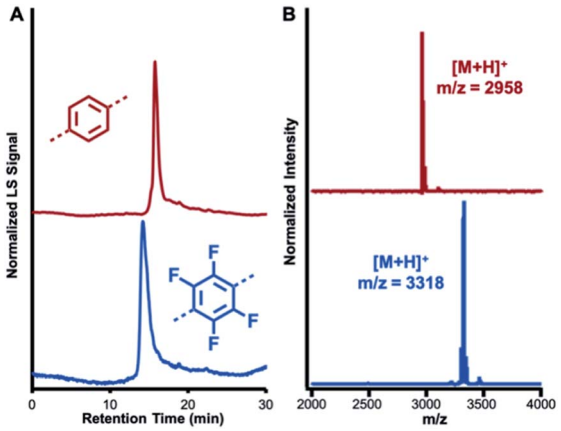

Fig. 2 Characterization of MC1 (red) and MC2 (blue). (A) SEC traces using a multi-angle light scattering (MALS) detector (B) MALDI-TOF MS spectra of MC1 and MC2.

adequate signal-to-noise, and this sample preparation also resulted in the appearance of low-intensity resonances, which we assign as small amounts of ring-opened oligomeric side-products. We attribute the appearance of these oligomers to the conditions needed to fully solvate the macrocycle for NMR spectroscopy because characterization of **MC2** by SEC and MALDI-MS prior to sonication did not show evidence of these linear products. However, MALDI-TOF MS performed after sonication did show peaks corresponding to linear oligomers (Fig. S9†). Taken together, these data demonstrate that **MC1** and **MC2** are formed efficiently and isolated in high purity, which enabled further study of their assembly and co-assembly.

Protonation of the pyridine groups within **MC1**, **MC2**, and a system prepared from a 1 : 1 mixture of both macrocycles induce their assembly into crystalline nanotubes (**NT1**, **NT2**, and **NT3**, respectively), as evaluated by *in solvo* synchrotron XRD and AFM, Fig. 3. After allowing the macrocyclization reaction to equilibrate for 24 h, the resulting gel was placed into a capillary tube and subjected to synchrotron *in solvo* XRD measurements. The assembly of macrocycles prepared from **1** into nanotubes is characterized by the emergence of a diffraction feature between 0.11 and 0.12 $Å^{-1}$, corresponding to a macrocycle with an internal cavity of *ca.* 3.00 nm. For **NT1** this peak is observed at 0.12 $Å^{-1}$, along with the presence of higher order diffraction peaks, indicative of a highly crystalline material. Similarly, **NT2** demonstrated a diffraction feature at 0.11 $Å^{-1}$, confirming its assembly into nanotubes of a similar size and shape. **NT3** was prepared by suspending purified **MC1** and **MC2** in 1,4-dioxane and inducing assembly through the addition of CF_3CO_2H (1 equiv. per macrocycle). This acid loading ensures that the threshold for assembly is met,[20,21] while being sufficiently low to avoid free CF_3CO_2H that impedes nanotube processing by touch-spinning. **NT3** exhibits a prominent diffraction feature at 0.12 $Å^{-1}$, indicative of the formation of a crystalline material with similar periodicity as **NT1** and **NT2**. However, the full-width at half max of the ⟨100⟩ and the higher ordering scattering features is significantly decreased in the mixed system relative to either **NT1** or **NT2**, signifying enhanced crystallinity

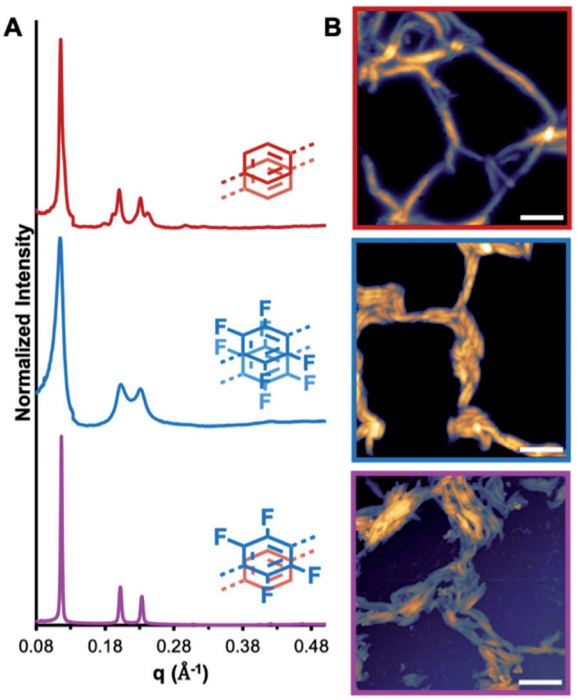

Fig. 3 Characterization of nanotubes prepared through macrocycle assembly. (A) *In solvo* synchrotron XRD patterns of NT1 (red), NT2 (blue), and NT3 (pink). (B) AFM images (2 μm scale bar) of NT1 (red), NT2 (blue), and NT3 (pink).

in the mixed macrocycle system. We attribute the enhanced crystallinity in this system to the formation of AP interactions that are not available to either of the parent systems. While *in solvo* XRD demonstrates macrocycle assembly, AFM of nanotube drop-cast solutions revealed that these assemblies are formed as high-aspect ratio structures with lengths on the order of microns. Aliquots of the mixtures were diluted and drop-cast onto a silicon wafer and imaged by AFM. In the case of **NT1**, nanotube bundles approximately 50 nm across are observed, while **NT2** formed larger, more uniform bundles from nanotubes ranging in diameter from 50 to 500 nm. **NT3** is observed as nanotube bundles approximately 500 nm in diameter are comprised of smaller nanotubes. Pyridinium ions are presumed to be the guiding factor in these assembly processes due to the enhanced basicity of the pyridines relative to the imines, and the inability for structurally similar macrocycles lacking pyridine groups to assemble under identical conditions.[35] Taken together, the emergence of strong diffraction signals and direct imaging observations highlight that **MC1**, **MC2**, and their mixed system assemble into high-aspect ratio nanotubes under mild conditions, thereby enabling further study into the effects of AP interactions on the mechanical strengths of mixed assemblies.

UV-Vis and fluorescence spectroscopy demonstrate that **NT3** exhibit spectral features associated with AP interactions. Macrocycle solutions (5 mM) in 1,4-dioxane were acidified with CF_3CO_2H (1 equiv. per macrocycle), diluted to 5 μM, and subjected to UV-Vis and fluorescence spectroscopy. In all cases, acid

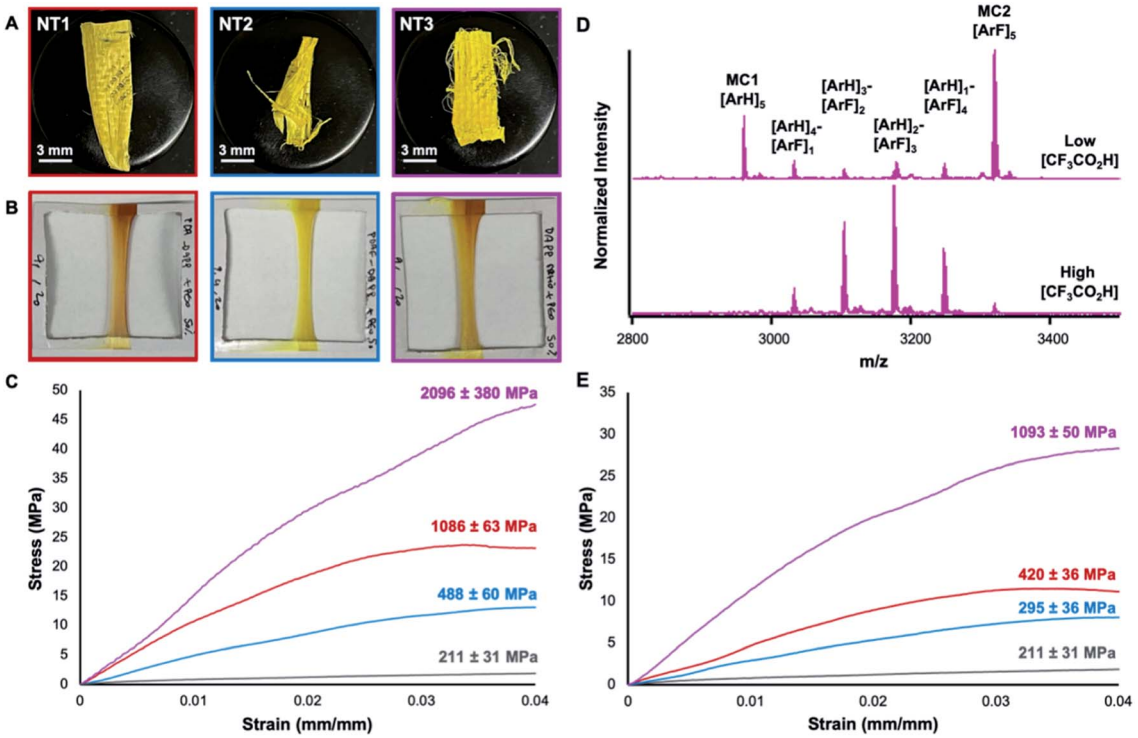

Fig. 4 Mechanical testing of touch-spun nanotube-loaded fibers. (A) Optical images of touch-spun nanotube-loaded fibers. (B) Optical images of mounted fibers before tensile testing. (C) Tensile stress–strain behavior of the touch-spun nanotube fibers formed from low acid loadings and a touch-spun PEO control sample (gray). (D) MALDI-TOF MS spectra of degraded **NT3** fibers depicting (top) low degrees of macrocycle scrambling in the presence of low acid concentrations and (bottom) statistical macrocycle scrambling in the presence of large excesses of CF_3CO_2H. (E) Tensile stress–strain behavior of the touch-spun nanotube fibers formed from higher acid loadings.

addition resulted in an increase in the emission intensity between 300 and 600 nm ($\lambda_{ex} = 340$ nm), which we attribute to a decreased number of non-radiative relaxation pathways in rigid molecular assemblies. The co-assembly of **MC1** and **MC2** exhibit the hallmarks of AP interactions in its fluorescence signature, specifically a 5-nm blue shift relative to the neutral macrocycle solutions ($\lambda_{ex} = 340$ nm) (Fig. S26†). The magnitude of this shift is consistent with previous reports on AP interactions that are induced without the formation of charge transfer complexes.[33,37] This shift was not observed in the spectra of **NT1** or **NT2** over the same period of time, further validating that the observed shift due to AP interactions ($\lambda_{ex} = 340$ nm, Fig. S22–S25†). Taken together, these data demonstrate that **NT3** is supported by additional AP interactions, not accessible in either **NT1** or **NT2**, and inspired studies into how these interactions could impact the mechanical strength of the assemblies.

Touch-spun nanofibers possessing nanotube assemblies demonstrated that AP interactions present in **NT3** persist when placed in composite fibers and lead to enhanced mechanical properties relative to fibers possessing nanotubes that lack such interactions. Solutions of **MC1**, **MC2**, and a stoichiometric 1 : 1 mixture of **MC1** : **MC2** in 1,4-dioxane (5 mM) were acidified with CF_3CO_2H (1 equiv. per macrocycle) and mixed with 1 wt% of poly(ethylene oxide) (PEO, $M_n = 4\,000\,000$ g mol^{-1}). The addition of PEO increases the viscosity of the nanotube solutions and affords the fabrication of nanofibers *via* touch spinning (Whiff LLC). In the touch-spinning process, nanotube solutions are pushed through a syringe pump, where droplets released from the tip form a liquid bridge with bars on a nearby rotating disc.[17] As the disc rotates and the polymer is stretched, the solvent evaporates rapidly to form fibers. Cross-sectional scanning electron microscopy (SEM) indicated the high uniformity of the fibers ($Ø = 8.8 \pm 0.6$ μm, 14 ± 1.3 μm, and 3.7 ± 0.3 μm for **NT1**, **NT2**, and **NT3**, respectively), (Fig. S35–S37†). The prepared fibers were then mounted and subjected to uniaxial tensile testing which revealed Young's modulus of 1086 ± 63 MPa (**NT1**, red) and 488 MPa ± 60 (**NT2**, blue) for assemblies lacking AP interactions. However, when present, AP interactions in touch-spun nanotube fibers resulted in a 93% increase in the Young's modulus (**NT3**: 2096 ± 380 MPa, pink) (Fig. 4C). The observed increase in the elastic modulus highlights the utility of AP interactions in enhancing the mechanical properties of supramolecular assemblies.

The macrocycles exhibited chemical stability through the assembly and touch-spinning process. After the touch-spinning process, intact, pure **MC1** and **MC2** were recovered from the nanotubes by dispersing the fibers in triethylamine, leading to deprotonation of the pyridinium moiety and macrocycle disassembly. The insoluble macrocycles were then recovered by centrifugation, and characterized by MALDI-TOF MS. **MC1** and **MC2** were recovered from **NT1** and **NT2** and were respectively

observed as the $[M + H]^+$ adduct at m/z 2959.35 and 3320.23 (Fig. S10–S11†). In samples of **NT3**, recovered **MC1** and **MC2** were observed as the corresponding $[M + H]^+$ adducts at m/z 2959.30 and 3319.04, respectively (Fig. 4D). MALDI-TOF MS of the macrocycles recovered from **NT3** also revealed minor peaks corresponding to small amounts of exchange of arene and perfluoroarene groups among **MC1** and **MC2** during the assembly, touch-spinning and/or recovery process. Given that **MC1** and **MC2** have similar mass spectrometry ionization efficiencies, these scrambled products are minor and not disruptive of assembly. Nevertheless, we set out to explore this exchange process and its impact on nanotube assembly by intentionally scrambling the macrocycles to a greater extent.

Nanotubes prepared from scrambled macrocycles bearing statistical distributions of **2** and **3** exhibited Young's moduli lower than **NT3**, but still greater than **NT1** or **NT2**. Intentionally scrambled species were prepared by mixing as-synthesized samples of **NT1** and **NT2** in a 1 : 1 ratio and equilibrating them with higher concentrations of CF_3CO_2H for 24 h. Neutralization of the scrambled system and analysis by MALDI-TOF MS demonstrated a statistical scrambling of both dialdehyde monomers, yielding four new macrocycles with varying perfluoro and perhydro subunits (Fig. 4D). Despite this scrambling, fibers touch-spun from the scrambled nanotubes exhibited a Young's modulus of 1093 ± 50 MPa, compared to 420 ± 36 and 295 ± 36 MPa obtained from **NT1** and **NT2** samples prepared under equally high acid concentrations, respectively (Fig. 4E). We attribute the enhanced mechanical strength in the scrambled species to the formation of many AP interactions even if not every structure can maximize the alternation of its aryl and perfluoroaryl groups. Taken together with the mechanical strengths of pure **NT3**, these data demonstrate how collective AP interactions are a powerful tool in tuning the mechanical properties of macrocycle assemblies and has resulted in the stiffest nanotubes to date. These findings will spur further research efforts into exploring additional non-covalent interactions to further enhance the mechanical properties of these nanotube assemblies.

Conclusions

Nanotubes prepared from the co-assembly of macrocycles bearing aromatic and perfluoroaromatic residues exhibit significantly enhanced Young's moduli compared to nanotubes lacking such interactions. A one pot synthesis of **NT1** and **NT2** occurs through condensation of **1** with either **2** or **3**, subsequent deprotonation leads to the isolation of **MC1** and **MC2**. A 50 : 50 mixture of **MC1** and **MC2** formed a mixed nanotube (**NT3**) with both arene and perfluoroarene subunits. We demonstrate the dual system's assembly through *in solvo* synchrotron XRD measurements, which demonstrate enhanced crystallinity within **NT3**, relative to **NT1** and **NT2**. Furthermore, AFM imaging of the mixed system revealed nanotube bundles approximately 500 nm in diameter. Fluorescence spectroscopy suggests AP interactions are present in **NT3** through a 5 nm blueshift upon assembly that is not present in either **NT1** or **NT2**. Touch-spinning the assemblies into fibers demonstrates their processability and also allows for uniaxial tensile testing, which reveals a Young's modulus of 2.096 GPa for **NT3**, a 93% increase from **NT1** (1.086 GPa). This direct comparison of AP and analogous non-AP systems demonstrates how beneficial leveraging secondary interactions such as AP interactions can be in supramolecular assemblies and offers the opportunity to further enhance the nanotubes mechanical strength through orthogonal non-covalent interactions.

Data availability

All characterization data is available in the ESI.† Raw data sets are available from the corresponding authors.

Author contributions

Conceptualization: EKR, DA, MJS, AME, MLB, WRD. Investigation: EKR, DA, AK. Methodology: EKR, DA, AK, MJS. Funding aquisition, supervision: MLB, WRD. Writing – original draft, writing – review and editing: all authors.

Conflicts of interest

The authors declare no competing financial interests.

Acknowledgements

E. K. R was supported by the Department of Energy (DOE) under grant no. (DE-SC0019356). M. L. B was supported by the National Science Foundation (NSF) under Grant No. (DMR 1507420). M. J. S was supported by the NSF through the Graduate Research Fellowship Program (GRFP) under Grant No. (DGE-1842165). M. J. S. is partially supported by the Ryan Fellowship and the International Institute for Nanotechnology. A. M. E. was supported by the NSF through the GRFP under Grant No. (DGE-1324585). This work made use of the Integrated Molecular Structure Education and Research Center (IMSERC) at Northwestern University, which has received support from the NSF (CHE-1048773), the Soft and Hybrid Nanotechnology Experimental (SHyNE) Resource (NSF; NNCI-1542205), the State of Illinois, and the International Institute for Nanotechnology (IIN). This work also made use of the Scanned Probe Imaging and Development (SPID), and the Electron Probe Instrumentation Center (EPIC), facilities of Northwestern University's Atomic and Nanoscale Characterization Experiment Center (NUANCE), which has received support from the Soft and Hybrid Nanotechnology Experimental (SHyNE) Resource (NSF; ECCS-1542205). This work was also supported by the Northwestern University Keck Biophysics Facility and a Cancer Center Support Grant (NCI CA060553). Parts of this work were performed at the DuPont-Northwestern-Dow Collaborative Access Team (DND-CAT) located at Sector 5 of the Advanced Photon Source (APS) at Argonne National Lab. This research used resources of the Advanced Photon Source and the Center for Nanoscale Materials, both U.S. Department of Energy (DOE) Office of Science User Facilities operated for the DOE Office of

Science by Argonne National Laboratory under Grant No. (DGE-1324585).

References

1 M. Fischer, G. Lieser, A. Rapp, I. Schnell, W. Mamdouh, S. De Feyter, F. C. De Schryver and S. Hoger, *J. Am. Chem. Soc.*, 2004, **126**, 214–222.
2 S. Iijima, *Nature*, 1991, **354**, 56–58.
3 K. Sato, Y. Itoh and T. Aida, *J. Am. Chem. Soc.*, 2011, **133**, 13767–13769.
4 T. Shimizu, W. Ding and N. Kameta, *Chem. Rev.*, 2020, **120**, 2347–2407.
5 M. Stepien, B. Donnio and J. L. Sessler, *Angew. Chem., Int. Ed.*, 2007, **46**, 1431–1435.
6 J. Zhang and J. S. Moore, *J. Am. Chem. Soc.*, 1994, **116**, 2655–2656.
7 N. Kameta, W. Ding and J. Dong, *ACS Omega*, 2017, **2**, 6143–6150.
8 N. Kameta, J. Dong and H. Yui, *Small*, 2018, **14**, e1800030.
9 A. J. Helsel, A. L. Brown, K. Yamato, W. Feng, L. Yuan, A. J. Clements, S. V. Harding, G. Szabo, Z. Shao and B. Gong, *J. Am. Chem. Soc.*, 2008, **130**, 15784–15785.
10 H. Xu, S. Nagasaka, N. Kameta, M. Masuda, T. Ito and D. A. Higgins, *Phys. Chem. Chem. Phys.*, 2016, **18**, 16766–16774.
11 H. Xu, S. Nagasaka, N. Kameta, M. Masuda, T. Ito and D. A. Higgins, *Phys. Chem. Chem. Phys.*, 2017, **19**, 20040–20048.
12 P. Beker, I. Koren, N. Amdursky, E. Gazit and G. Rosenman, *J. Mater. Sci.*, 2010, **45**, 6374–6378.
13 X. Xu, S. Chen, Y. Chen, H. Sun, L. Song, W. He and X. Wang, *Small*, 2016, **12**, 2982–2990.
14 Y. Xu, T. Wang, Z. He, A. Zhong, W. Yu, B. Shi and K. Huang, *Polym. Chem.*, 2016, **7**, 7408–7415.
15 J. Yang, M. B. Dewal and L. S. Shimizu, *J. Am. Chem. Soc.*, 2006, **128**, 8122–8123.
16 D. T. Bong, T. D. Clark, J. R. Granja and M. R. Ghadiri, *Angew. Chem., Int. Ed.*, 2001, **40**, 988–1011.
17 S. Dong, B. Zheng, F. Wang and F. Huang, *Acc. Chem. Res.*, 2014, **47**, 1982–1994.
18 X. Yan, F. Wang, B. Zheng and F. Huang, *Chem. Soc. Rev.*, 2012, **41**, 6042–6065.
19 C. Sun, M. Shen, A. D. Chavez, A. M. Evans, X. Liu, B. Harutyunyan, N. C. Flanders, M. C. Hersam, M. J. Bedzyk, M. Olvera de la Cruz and W. R. Dichtel, *Proc. Natl. Acad. Sci. U.S.A.*, 2018, **115**, 8883–8888.
20 M. J. Strauss, D. Asheghali, A. M. Evans, R. L. Li, A. D. Chavez, C. Sun, M. L. Becker and W. R. Dichtel, *Angew. Chem., Int. Ed.*, 2019, **58**, 14708–14714.
21 M. J. Strauss, M. Jia, A. M. Evans, I. Castano, R. L. Li, X. Aguilar-Enriquez, E. K. Roesner, J. L. Swartz, A. D. Chavez, A. E. Enciso, J. F. Stoddart, M. Rolandi and W. R. Dichtel, *J. Am. Chem. Soc.*, 2021, **143**(21), 8145–8153.
22 L. M. Salonen, M. Ellermann and F. Diederich, *Angew. Chem., Int. Ed.*, 2011, **50**, 4808–4842.
23 S. S. Babu, V. K. Praveen, S. Prasanthkumar and A. Ajayaghosh, *Chem. –Eur. J.*, 2008, **14**, 9577–9584.
24 K. B. Woody, J. E. Bullock, S. R. Parkin and M. D. Watson, *Macromolecules*, 2007, **40**, 4470–4473.
25 H. X. Wu, B. B. Ni, C. Wang, F. Zhai and Y. G. Ma, *Soft Matter*, 2012, **8**, 5486–5492.
26 R. Xu, B. Schweizer and H. Frauenrath, *J. Am. Chem. Soc.*, 2008, **130**, 11437–11445.
27 C. Y. Dai, P. Nguyen, T. B. Marder, A. J. Scott, W. Clegg and C. Viney, *Chem. Commun.*, 1999, 2493–2494, DOI: 10.1039/a906199a.
28 M. Weck, A. R. Dunn, K. Matsumoto, G. W. Coates, E. B. Lobkovsky and R. H. Grubbs, *Angew. Chem., Int. Ed.*, 1999, **38**, 2741–2745.
29 R. E. Yardley, J. A. Paquette, H. Taing, H. M. Gaebler, S. H. Eichhorn, I. P. Hamilton and K. E. Maly, *Org. Lett.*, 2019, **21**, 10102–10105.
30 A. F. Kilbinger and R. H. Grubbs, *Angew. Chem., Int. Ed.*, 2002, **41**, 1563–1566.
31 K. P. Castro, E. V. Bukovsky, I. V. Kuvychko, N. J. DeWeerd, Y. S. Chen, S. H. M. Deng, X. B. Wang, A. A. Popov, S. H. Strauss and O. V. Boltalina, *Chem. –Eur. J.*, 2019, **25**, 13547–13565.
32 Y. Q. Sun, Y. L. Lei, L. S. Liao and W. P. Hu, *Angew. Chem., Int. Ed.*, 2017, **56**, 10352–10356.
33 H. W. Zhang, J. L. Han, X. Jin and P. F. Duan, *Angew. Chem., Int. Ed.*, 2021, **60**, 4575–4580.
34 X. H. Zhou, J. D. Luo, S. Huang, T. D. Kim, Z. W. Shi, Y. J. Cheng, S. H. Jang, D. B. Knorr, R. M. Overney and A. K. Y. Jen, *Adv. Mater.*, 2009, **21**, 1976–1981.
35 A. D. Chavez, A. M. Evans, N. C. Flanders, R. P. Bisbey, E. Vitaku, L. X. Chen and W. R. Dichtel, *Chem. –Eur. J.*, 2018, **24**, 3989–3993.
36 M. J. Strauss, A. M. Evans, I. Castano, R. L. Li and W. R. Dichtel, *Chem. Sci.*, 2020, **11**, 1957–1963.
37 A. Mandal, A. Choudhury, P. K. Iyer and P. Mal, *J. Phys. Chem. C*, 2019, **123**, 18198–18206.